AGU ADVANCING EARTH AND SPACE SCIENCES

Geophysical Research Letters®

Correspondence to:

Q. Ni,
niqinbiao@outlook.com

Full-Depth Eddy Kinetic Energy in the Global Ocean Estimated From Altimeter and Argo Observations

Qinbiao Ni[1,2,3] ⓘ, **Xiaoming Zhai**[2] ⓘ, **J. H. LaCasce**[4] ⓘ, **Dake Chen**[1,3] ⓘ, and **David P. Marshall**[5] ⓘ

[1]Southern Marine Science and Engineering Guangdong Laboratory (Zhuhai), Zhuhai, China, [2]School of Environmental Sciences, Centre for Ocean and Atmospheric Sciences, University of East Anglia, Norwich, UK, [3]State Key Laboratory of Satellite Ocean Environment Dynamics, Second Institute of Oceanography, Ministry of Natural Resources, Hangzhou, China, [4]Department of Geosciences, University of Oslo, Oslo, Norway, [5]Department of Physics, University of Oxford, Oxford, UK

Abstract Although the surface eddy kinetic energy (EKE) has been well studied using satellite altimeter and surface drifter observations, our knowledge of EKE in the ocean interior is much more limited due to the sparsity of subsurface current measurements. Here we develop a new approach for estimating EKE over the full depth of the global ocean by combining 20 years of satellite altimeter and Argo float data to infer the vertical profile of eddies. The inferred eddy profiles are surface-intensified at low latitudes and deep-reaching at mid- and high latitudes. They compare favorably to the first empirical orthogonal function obtained from current meter velocities. The global-integrated EKE estimated from the inferred profiles is about 3.1×10^{18} J, which is close to that estimated from the surface mode (3.0×10^{18} J) but about 30% smaller than that estimated from the traditional flat bottom modes (4.6×10^{18} J).

Plain Language Summary The ocean is full of mesoscale eddies, analogous to weather systems in the atmosphere. Eddy kinetic energy in the surface ocean is generally well studied thanks to the availability of satellite and drifter data. The subsurface eddy energy, on the other hand, is not well known due to the relative lack of subsurface current observations. Using vertical eddy structures inferred from satellite altimeter and Argo float data, we provide the first observational estimate of eddy kinetic energy over the full depth of the global ocean. Our results have important implications for understanding the ocean energy budget and for representing the effects of mesoscale eddies in ocean and climate models.

1. Introduction

Satellite altimetry reveals that the surface ocean is strongly turbulent, populated with mesoscale eddies from tens to hundreds of kilometers in size. These are generated by barotropic and baroclinic instabilities of the large-scale flow (Chelton et al., 2011; Gill et al., 1974; Ni, Zhai, Wang, & Hughes, 2020). These eddies dominate the ocean's kinetic energy spectrum and play a crucial role in transporting climatically important properties such as mass, heat, and carbon (Conway et al., 2018; Ni, Zhai, Wang, & Marshall, 2020; Wunsch, 1999; Zhai et al., 2010; Zhang et al., 2014).

A key metric commonly used to measure the strength of mesoscale eddies is the eddy kinetic energy (EKE). Diagnosing and characterizing global EKE from observations is important not only for understanding the ocean energy budget, but also for developing mesoscale eddy parameterizations for ocean and climate models. Such parameterizations often require solving an explicit eddy energy budget to determine the magnitude of eddy transfer coefficients (e.g., Eden & Greatbatch, 2008; Mak et al., 2018, 2022; Marshall & Adcroft, 2010; Marshall et al., 2012). One of the unknowns is the vertical structure of the eddy energy. Although the surface EKE in the global ocean has been well studied using geostrophic velocity anomalies derived from satellite altimeter and surface drifter data (Stammer, 1997; Wunsch & Stammer, 1998; Yu et al., 2019), the subsurface EKE remains poorly characterized and understood due to the limited spatio-temporal coverage of direct current observations in the ocean interior (de La Lama et al., 2016; Wunsch, 1997).

One way to estimate the full-depth EKE is to project altimeter-inferred surface geostrophic currents downward in the water column, which requires knowledge of the vertical structure of the eddies. It is common to use linear dynamical modes to deduce vertical eddy modal structures from the climatological ocean density field, for example, the barotropic mode and first baroclinic modes for a flat-bottomed ocean (Wunsch, 1997) and, more recently, the surface mode, which assumes vanishing bottom velocity (de La Lama et al., 2016; LaCasce, 2017).

However, given the assumptions and uncertainties associated with these dynamical mode methods, the applicability of using vertical mode structures to estimate full-depth EKE on a global scale is not clear. On the other hand, the global array of Argo profiling floats has collected vertical profiles of temperature and salinity in the upper 2,000 m of the global ocean for more than two decades. Combining millions of Argo float observations with concurrent altimeter data potentially provides a novel way of deriving the vertical structure of ocean eddies (Mulet et al., 2012; Ni, Zhai, Wang, & Hughes, 2020; Wunsch, 2008), which can then be used to estimate the full-depth EKE and compare with the results obtained from the dynamical mode approach.

2. Data Processing

The daily 1/4° × 1/4° altimetric sea level anomaly (SLA) data provided by Copernicus Marine Environment Monitoring Service used here span a 20-year period from 1998 to 2017. Each SLA map is spatially filtered using a high-pass Gaussian function (Chelton et al., 2011; Ni, Zhai, Wang, & Hughes, 2020; Xu et al., 2016)

$$G(k, l) = 1 - e^{-\frac{k^2 + l^2}{2\sigma^2}}, \tag{1}$$

where k and l are wavenumbers in the zonal and meridional directions, respectively, and the standard deviation σ corresponds to a half-power cutoff wavelength of 20°. This cutoff threshold removes the majority of large-scale signals related to heating/cooling and wind forcing but preserves mesoscale signals associated with the eddies (Figure S1 in Supporting Information S1).

The Argo float profiles that pass the quality control are obtained from the China Argo Real-time Data Center for the same 20-year period. For each Argo profile, potential density is calculated from temperature and salinity measurements and linearly interpolated in the depth range of 10–1,800 m at an interval of 10 m. The potential density anomaly (ρ') associated with mesoscale eddies is obtained by subtracting from an Argo profile a local climatological profile. This climatological profile is computed from averaging all the Argo profiles inside a bin of 5° × 5° (and collected within 45 days in each calendar year) centered at the profile under consideration (Ni et al., 2021; Zhang et al., 2013). The eddy pressure anomaly (P') is then calculated by integrating the hydrostatic equation downward from the surface (Mulet et al., 2012; Ni, Zhai, Wang, & Hughes, 2020; Wunsch, 2008):

$$P' = \rho_{\text{top}} g\eta + \int_z^0 \rho' g\, dz, \tag{2}$$

where ρ_{top} is the shallowest density record of an Argo profile, g is gravity, and η is the SLA at the location of the profile. The approach of integrating the hydrostatic equation downward from the surface is preferred compared to integrating upward from a hypothetical level of no motion, as many eddies are deep-reaching (e.g., Adams et al., 2011; Petersen et al., 2013; van Aken et al., 2003).

The World Ocean Atlas 2018 (WOA18) climatological hydrological data, provided by the U.S. National Centers for Environmental Information with a spatial resolution of 1°, are used to extrapolate vertical eddy structures in the deep ocean as well as calculate the linear dynamical modes. Current meter records are obtained from the U.S. National Centers for Environmental Information during the period from 1962 to 2005. These data are used to deduce the empirical orthogonal function (EOF) modes of the subsurface currents. Following de La Lama et al. (2016), the time series of the current velocity records are low-pass filtered with a Butterworth filter to remove periods shorter than 1 day. After that, we select only current-meter moorings that satisfy the following three criteria: (a) The mooring contains instruments at least at three different depths, (b) the records are longer than 90 days, and (c) the top instrument is located at a depth shallower than 1,500 m and the bottom instrument deeper than 3,000 m.

3. Composite Eddy Structures

Mesoscale eddies are first identified from the high-pass-filtered SLA maps using an eddy detection method based on SLA geometry (Chelton et al., 2011; Ni, Zhai, Wang, & Hughes, 2020; Ni, Zhai, Wang, & Marshall, 2020). In total, about 29 million eddy snapshots are identified in the global ocean over the 20-year period. Then, over 1 million pressure anomaly profiles are calculated from Argo floats located inside and around the eddies; these are used to obtain the vertical eddy structures via composite analysis (Chaigneau et al., 2011; Ni, Zhai, Wang, &
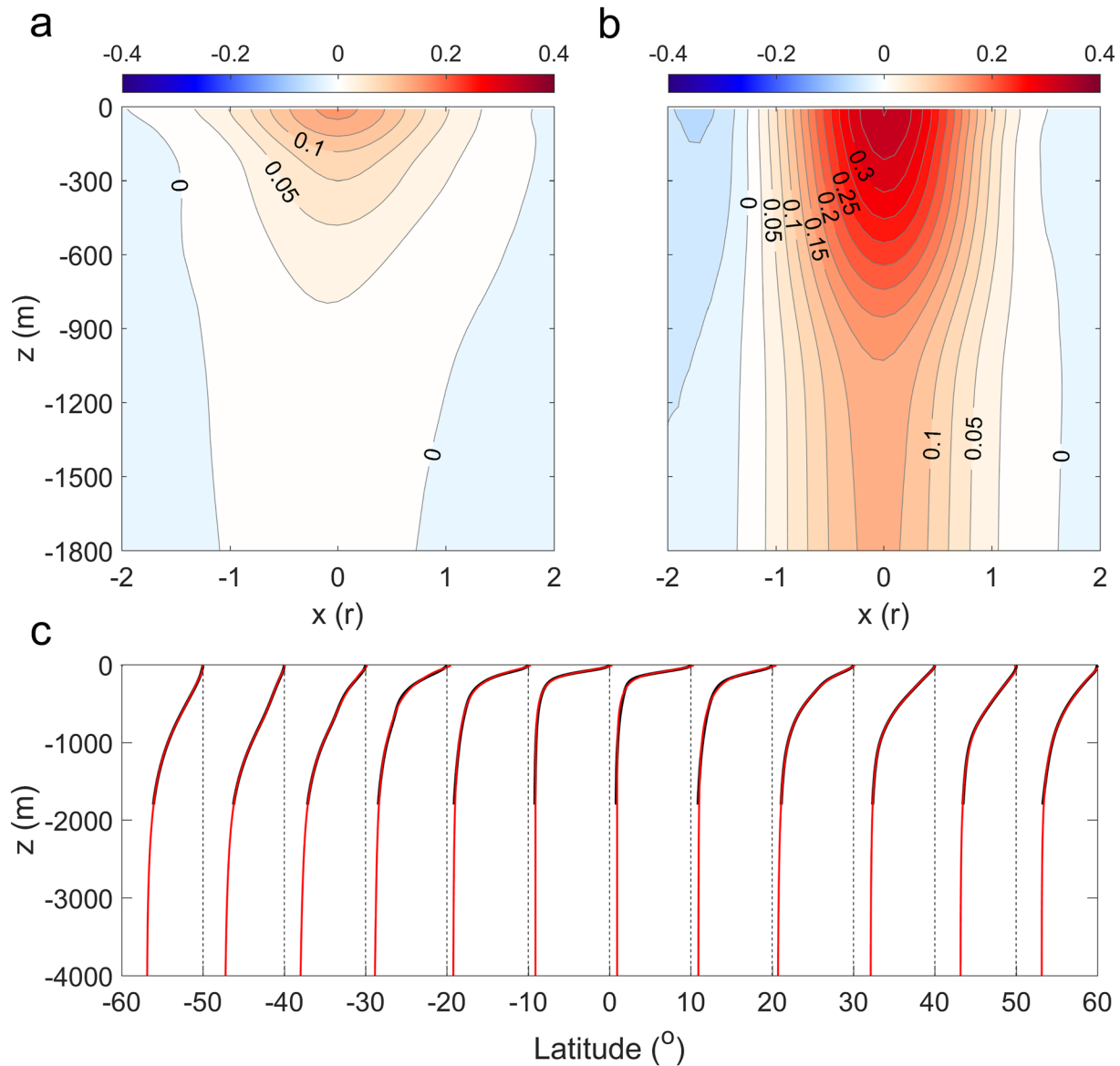
Figure 1. Vertical sections of pressure anomalies (dbar) at $y = 0$ associated with the composite eddies in (a) the Northwestern Subtropical Pacific Ocean and (b) the Gulf Stream. (c) Vertical pressure anomaly profiles (black curves) averaged within one eddy radius (r) from the eddy centers and normalized by the surface values for every 10° of latitude. The red curves show best-fit exponentials. Note that Argo profiles located within 5° of the Equator are excluded from the composite analysis.

Hughes, 2020; Ni et al., 2021). Note that the signs of the pressure anomaly profiles associated with cyclonic eddies are reversed before the composite analysis, since both types of eddies have similar shapes (Zhang et al., 2013). A detailed description of eddy identification and composite analysis methods is provided in the Supporting Information S1. We then composite the vertical eddy structures on a global 2° × 2° grid using 10° × 10° bins centered at each grid point. A bin size of 10° × 10° is used to ensure that there are sufficient Argo float profiles for the analysis at each grid point (Figure S2 in Supporting Information S1).

Consider the Northwestern Subtropical Pacific Ocean region (NSPO; [135°–145°E, 15°–25°N]) and the Gulf Stream region (GS; [51°–61°W, 31°–41°N]), where marked differences occur in the vertical structures of composite eddies (Figures 1a and 1b). The magnitude of eddy surface pressure anomaly in the NSPO region (~0.15 dbar) is only about half that in the GS region (~0.33 dbar). Furthermore, the composite eddy in the NSPO region displays a surface-intensified bowl-shaped vertical structure, with the pressure anomaly decreasing rapidly with depth, in line with the shallow eddy density anomaly (Figure S3a in Supporting Information S1). In contrast, the composite eddy in the GS region shows a funnel-shaped vertical structure, consistent with a deep-reaching

eddy density anomaly (Figure S3b in Supporting Information S1). Similar eddy structures have been reported previously from in-situ current observations (e.g., De Mey & Robinson, 1987; de Ruijter et al., 2002; Martin et al., 1998; van Aken et al., 2003; Wunsch, 1997). To assess the robustness of these structures obtained through downward integration of the hydrostatic equation using altimeter and Argo data, we made a similar analysis in the GS region in two different ways using HYbrid Coordinate Ocean Model reanalysis output; this yielded very similar results (Supporting Information S1, Figure S4).

Figure 1c shows the latitudinal variations of the composite vertical eddy structures, obtained by averaging pressure anomalies of the composite eddies within one eddy radius from the eddy centers in 10° latitude bands. These vertical structures, normalized by their surface values, decay monotonically with depth in the upper 1,800 m where Argo float data exist (black curves), consistent with previous research (Ni, Zhai, Wang, & Hughes, 2020; Zhang et al., 2013). We then apply an exponential function to fit the normalized structure in each 10° latitude band and extrapolate these vertical eddy structures to the deep ocean using a stretched vertical coordinate $z_s = \int_{-H}^{0} N/f\,dz$, where N is the buoyancy frequency estimated from WOA18, f is the Coriolis parameter and H is the depth of ocean bottom. Figure 1c shows that the best-fitting exponential function resembles very well the composite profile in the upper 1,800 m in all latitude bands. The eddy vertical structures are significantly surface-intensified at low latitudes but deep-reaching at mid- and high latitudes. Note too that composite profiles generally do not change sign with depth.

4. Comparison With First EOF Mode

Previous studies (e.g., de la Lama et al., 2016; Müller & Siedler, 1992) have shown that the first EOF mode captures a substantial fraction of the subsurface velocity variance, often exceeding 80% at current meter locations. As a further check, we compare the vertical structures with the first EOFs obtained from 144 current meter moorings located 5° poleward of the Equator that pass the selection criteria (see Section 2). Figure 2a shows the global distribution of the moorings, which are most abundant in the Atlantic Ocean. We obtain the first EOF mode at each mooring (see Supporting Information S1) and then average the EOF modes separately for the 39 selected current meter moorings located at low latitudes (<30°) and 105 current meter moorings at high latitudes (>30°). The averaged first EOF modes (black curves in Figure 2) are found to decay monotonically with depth and then remain relatively constant below about 1,500 m at low latitudes and below about 2,000 m at high latitudes, exhibiting a funnel-shaped structure. Note that on most moorings the uppermost current meter is typically positioned a few hundred meters below the sea surface; the extrapolation of EOFs to the sea surface is not straightforward (Wunsch, 1997).

We then composite the vertical eddy structure (red curves) using only Argo float data within a circle of a radius of 2.5° centered at the location of each mooring and extrapolate below 1,800 m depth using the exponential fit. The resulting vertical eddy structure closely resembles the average first EOF mode at both low and high latitudes. We also derive the linear surface mode (blue curves) and first baroclinic mode (orange curves) using the WOA18 climatological density profiles at the locations of current moorings (Supporting Information S1). Compared with the first EOF mode, the surface mode decreases more slowly with depth in the upper ocean and more quickly in the deep ocean, although it lies within one standard deviation of the first EOF modes. The more rapid attenuation of the surface mode in the deep ocean is probably due to the assumption of zero bottom velocities, together with the absence of a bottom boundary layer (LaCasce, 2017). By contrast, the first baroclinic mode decays much faster with depth than the first EOF mode and switches sign at ∼1,500 m. Our EOF analysis of current meter data thus shows that deducing vertical eddy structures from a combination of altimeter and Argo float data provides a promising way of projecting surface currents downward in the water column to obtain the full-depth horizontal eddy velocities.

5. Full-Depth EKE

To estimate the global time-mean EKE over the full water depth, we first derive the surface geostrophic current velocities from the high-pass-filtered SLA maps assuming geostrophic balance (Ni, Zhai, Wang, & Hughes, 2020). The surface EKE is calculated from

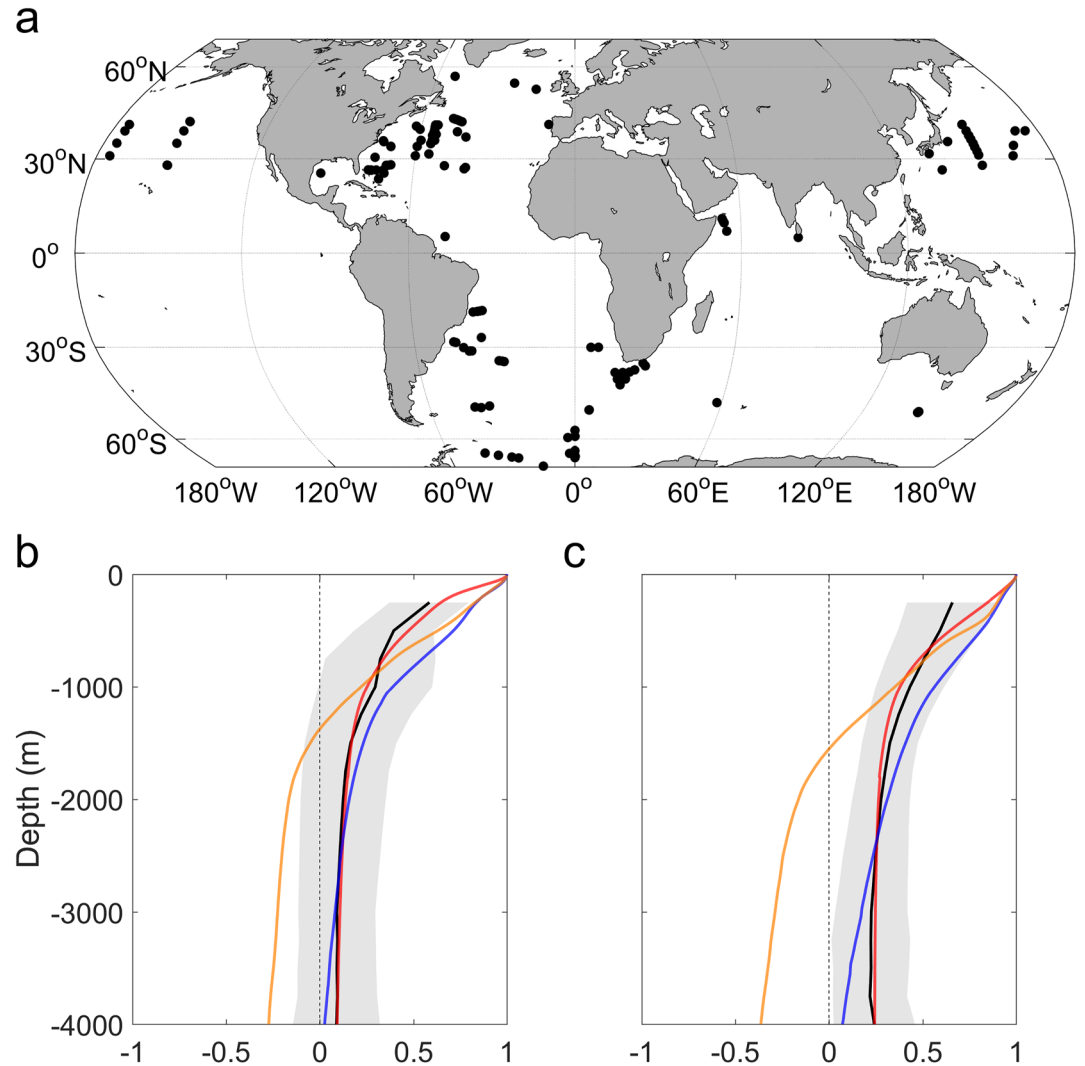$$EKE_0 = \frac{u_0^2 + v_0^2}{2},$$ (3)

Figure 2. (a) Locations of the selected current-meter moorings in the global ocean. (b) Mean (black curve) and one standard deviation (gray shading) of the first empirical orthogonal function modes derived from the current meter moorings located at latitudes lower than 30° in panel (a). The red curve shows the vertical eddy structure composited using the Argo data inside a circle with a radius of 2.5° centered at each mooring. Note that the eddy structure below 1,800 m of the red line is obtained by the exponential fit. The blue and orange curves show the averages of the surface modes and first baroclinic modes at the mooring locations, respectively. (c) As panel (b) but for latitudes higher than 30°.

where u_0 and v_0 are the zonal and meridional components of surface geostrophic currents, respectively. The surface geostrophic velocities are then projected downward using the estimated vertical eddy structures to obtain the subsurface geostrophic velocities:

$$u(z) = u_0 \cdot F(z), \tag{4}$$

$$v(z) = v_0 \cdot F(z), \tag{5}$$

where $F(z)$ is the vertical eddy structure normalized by its surface value in each bin and z is the depth. Note that the composite (black curves in Figure 1c) and extrapolated (red curves in Figure 1c) eddy structures are used for depths above and below 1,800 m, respectively. Combining Equations 3–5, EKE over the whole water column can be estimated by

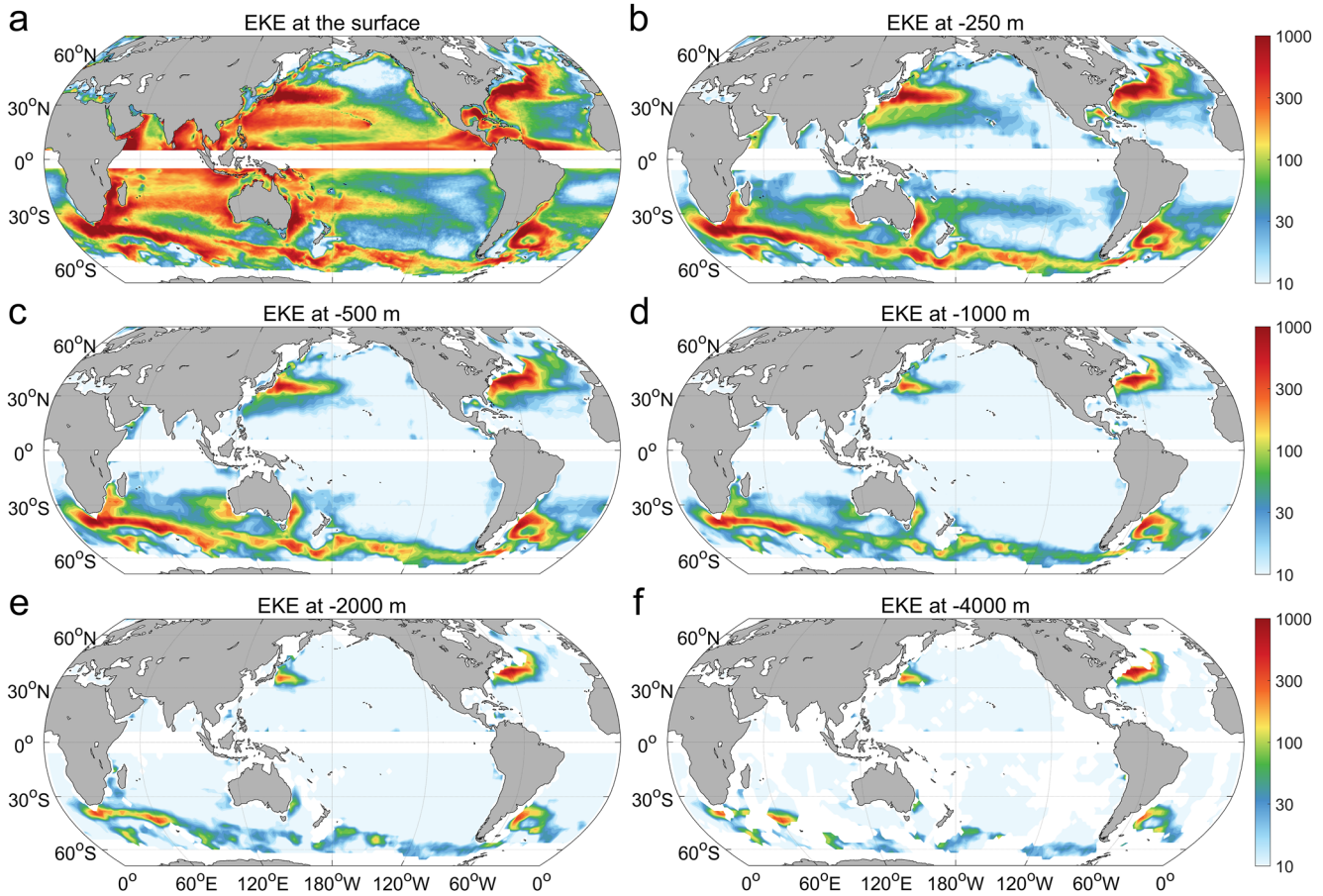$$\overline{\text{EKE}(z)} = \overline{\text{EKE}_0} \cdot F(z)^2, \tag{6}$$

Figure 3. Global distributions of eddy kinetic energy (cm² s⁻²) estimated using the altimeter and Argo observations at (a) the surface and at (b) −250 m, (c) −500 m, (d) −1,000 m, (e) −2,000 m, and (f) −4,000 m.

where the overbars indicate the time mean. Figure 3 shows that the spatial patterns of EKE at different depths resemble that at the surface (as they must), with large values near the western boundary currents and the Antarctic Circumpolar Current. The EKE is O (1000) cm² s⁻² at the surface and can reach O (100) cm² s⁻² even at 4,000 m depth in these strong current regions, while it is rather small below 500 m in the rest of the ocean. The hotspots of high EKE in the deep ocean of the western boundary current and the Antarctic Circumpolar Current regions suggest potentially elevated eddy energy dissipation rates there as a result of eddy-topography interaction (Yang et al., 2021).

For comparison, we apply the linear baroclinic modes to estimate the full-depth EKE in the global ocean. These are derived from the WOA18 climatological density field (Supporting Information S1; LaCasce, 2017; LaCasce & Groeskamp, 2020). We calculate both the standard (flat bottom) baroclinic modes and the surface modes (with zero flow at the bottom) and use both to project the surface EKE downward into the ocean interior. For the flat bottom modes, we assume that (a) EKE in the ocean is dominated and approximately equipartitioned by the barotropic and first baroclinic modes and (b) altimeter data reflects mostly the first baroclinic mode in the open ocean, following Wunsch (1997).

Figure 4 shows the depth-integrated EKE $\int_{-H}^{0} \rho_0 \cdot \overline{EKE(z)} \cdot dz$ (where H is the depth of the ocean and ρ_0 is the reference density) estimated from the three approaches. The overall large-scale spatial patterns are similar, with elevated EKE levels in the western boundary current and the Antarctic Circumpolar Current regions. However, the magnitude of the depth-integrated EKE estimated based on the traditional flat bottom modes is significantly greater than those estimated from the other two approaches. The global-integrated EKE estimated from the composite eddy structures is about 3.1×10^{18} J, which is close to that estimated based on the surface mode (3.0×10^{18} J) but about one-third smaller than that estimated from the flat bottom modes (4.6×10^{18} J).
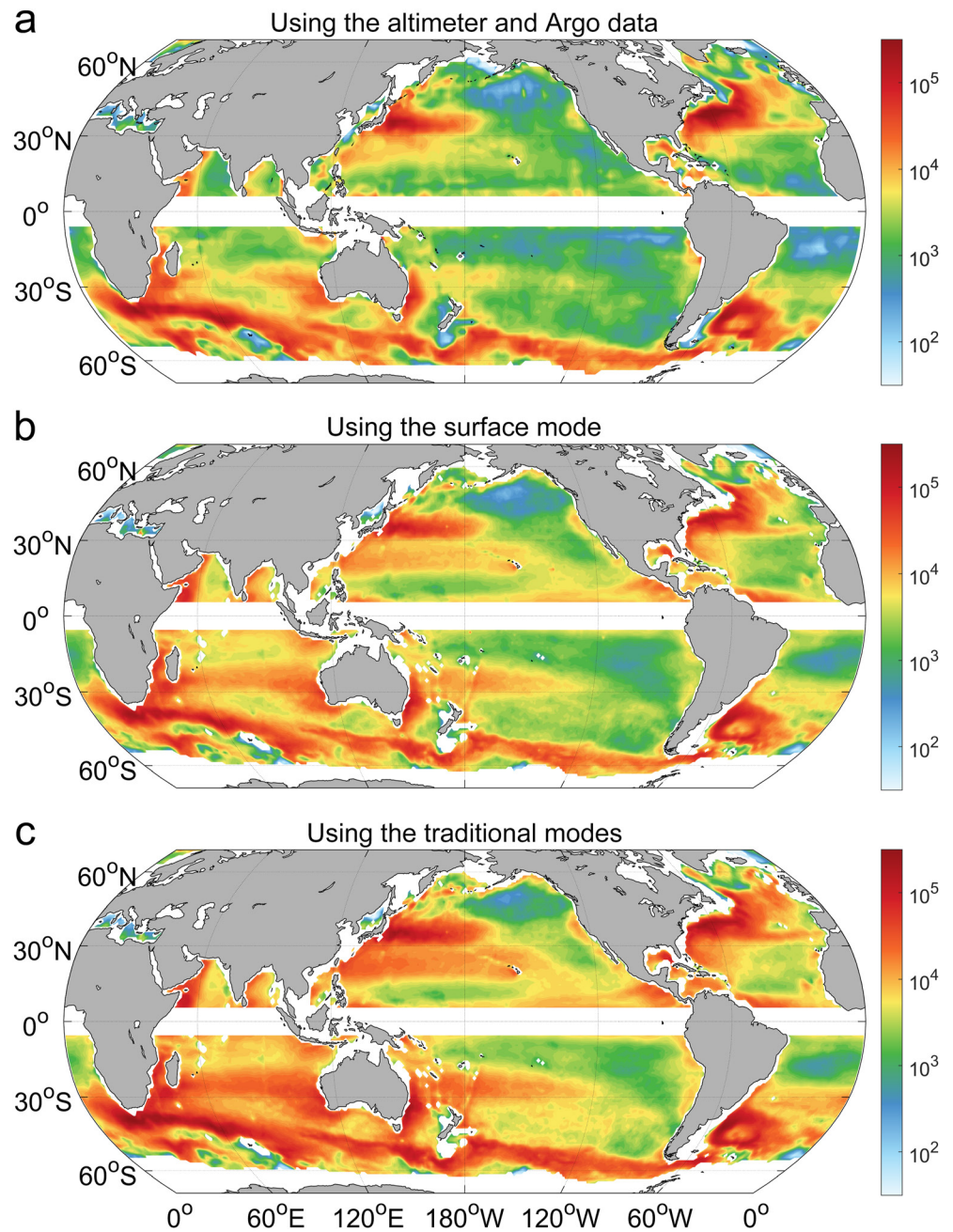
Figure 4. Global patterns of depth-integrated eddy kinetic energy (J m^{-2}) estimated from (a) the altimeter and Argo data, (b) the surface mode, and (c) the barotropic and first baroclinic modes.

6. Conclusions

Based on satellite altimeter and Argo float observations over two decades (1998–2017), we provide the first estimate of full-depth EKE in the global ocean. The vertical eddy structures obtained from composite analysis of altimeter and Argo data are surface-intensified at low latitudes but deep-reaching at mid- and high latitudes. These vertical eddy structures closely resemble the first EOF modes and thus offer a promising new means of projecting surface currents downward in the water column to obtain the full-depth horizontal eddy velocities. The resulting EKE is large at all depths near the western boundary currents and the Antarctic Circumpolar Current, with a global total of about 3.1×10^{18} J.

Given the importance of EKE for the ocean circulation, tracer transport and energy cascades (Ferrari & Wunsch, 2010), our full-depth estimates have important implications for understanding the ocean energy budget as well as for developing energetically-consistent eddy parameterization schemes (Eden & Greatbatch, 2008; Mak et al., 2018; Marshall & Adcroft, 2010; Marshall et al., 2012). Furthermore, the newly-estimated full-depth EKE provides a new reference for validating eddy-permitting and eddy-resolving ocean models, moving beyond the current standard practice of comparing model-simulated surface EKE with those derived from altimeter and drifter data (Rieck et al., 2015; Scott et al., 2010; Yu et al., 2019). Future improvements of the full-depth EKE estimates will benefit from continuous deployment of Argo profiling floats, including deep Argo floats that profile down to near the sea floor, particularly in regions where the current numbers of Argo floats are low.

Data Availability Statement

All the data used in this study are publicly available. The satellite altimeter data are available at https://data.marine.copernicus.eu/product/SEALEVEL_GLO_PHY_L4_MY_008_047/description, the Argo float data are available at https://argo.ucsd.edu/links/#National, the WOA18 climatological data are available at https://www.nodc.noaa.gov/OC5/woa18/woa18data.html, the current meter data are available at https://www.ncei.noaa.gov/access/data/global-ocean-currents-database/cmportal.html and the reanalysis data from the HYCOM simulation are available at http://tds.hycom.org/thredds/catalog.html.

References

Adams, D. K., McGillicuddy, D. J., Zamudio, L., Thurnherr, A. M., Liang, X., Rouxel, O., et al. (2011). Surface-generated mesoscale eddies transport deep-sea products from hydrothermal vents. *Science*, *332*(6029), 580–583. https://doi.org/10.1126/science.1201066

Chaigneau, A., Texier, M. L., Eldin, G., Grados, C., & Pizarro, O. (2011). Vertical structure of mesoscale eddies in the eastern South Pacific Ocean: A composite analysis from altimetry and Argo profiling floats. *Journal of Geophysical Research*, *116*, C11025.

Chelton, D. B., Schlax, M. G., & Samelson, R. M. (2011). Global observations of nonlinear mesoscale eddies. *Progress in Oceanography*, *91*(2), 167–216. https://doi.org/10.1016/j.pocean.2011.01.002

Conway, T. M., Palter, J. B., & de Souza, G. F. (2018). Gulf Stream rings as a source of iron to the North Atlantic subtropical gyre. *Nature Geoscience*, *11*(8), 594–598. https://doi.org/10.1038/s41561-018-0162-0

de La Lama, M. S., Lacasce, J. H., & Kristine, F. H. (2016). The vertical structure of ocean eddies. *Dynamics & Statistics of the Climate System*, *1*(1), 1–16.

De Mey, P., & Robinson, A. R. (1987). Assimilation of altimeter eddy fields in a limited-area quasi-geostrophic model. *Journal of Physical Oceanography*, *17*(12), 2280–2293. https://doi.org/10.1175/1520-0485(1987)017<2280:aoaefi>2.0.co;2

de Ruijter, W. P. M., Ridderinkhof, H., Lutjeharms, J. R. E., Schouten, M. W., & Veth, C. (2002). Observations of the flow in the Mozambique Channel. *Geophysical Research Letters*, *29*(10), 140-1–140-3. https://doi.org/10.1029/2001gl013714

Eden, C., & Greatbatch, R. J. (2008). Towards a mesoscale eddy closure. *Ocean Modelling*, *20*(3), 223–239. https://doi.org/10.1016/j.ocemod.2007.09.002

Ferrari, R., & Wunsch, C. (2010). The distribution of eddy kinetic and potential energies in the global ocean. *Tellus*, *62*, 92–108. https://doi.org/10.3402/tellusa.v62i2.15680

Gill, A. E., Green, J. S. A., & Simmons, A. J. (1974). Energy partition in the large-scale ocean circulation and the production of mid-ocean eddies. *Deep Sea Research*, *21*(7), 499–528. https://doi.org/10.1016/0011-7471(74)90010-2

LaCasce, J. H. (2017). The prevalence of oceanic surface modes. *Geophysical Research Letters*, *44*(21), 11097–11105. https://doi.org/10.1002/2017gl075430

LaCasce, J. H., & Groeskamp, S. (2020). Baroclinic modes over rough bathymetry and the surface deformation radius. *Journal of Physical Oceanography*, *50*(10), 1–40. https://doi.org/10.1175/jpo-d-20-0055.1

Mak, J., Maddison, J. R., Marshall, D. P., & Munday, D. R. (2018). Implementation of a geometrically informed and energetically constrained mesoscale eddy parameterization in an ocean circulation model. *Journal of Physical Oceanography*, *48*(10), 2363–2382. https://doi.org/10.1175/jpo-d-18-0017.1

Mak, J., Marshall, D. P., Madec, G., & Maddison, J. R. (2022). Acute sensitivity of global ocean circulation and heat content to eddy energy dissipation timescale. *Geophysical Research Letters*, *49*(8), e2021GL097259. https://doi.org/10.1029/2021gl097259

Marshall, D. P., & Adcroft, A. (2010). Parameterization of ocean eddies: Potential vorticity mixing, energetics and Arnold's first stability theorem. *Ocean Modelling*, *32*(3–4), 188–204. https://doi.org/10.1016/j.ocemod.2010.02.001

Marshall, D. P., Maddison, J. R., & Berloff, P. S. (2012). A framework for parameterizing eddy potential vorticity fluxes. *Journal of Physical Oceanography*, *42*(4), 539–557. https://doi.org/10.1175/jpo-d-11-048.1

Martin, A. P., Wade, I. P., Richards, K. J., & Heywood, K. J. (1998). The PRIME eddy. *Journal of Marine Research*, *56*(2), 439–462. https://doi.org/10.1357/002224098321822375

Mulet, S., Rio, M. H., Mignot, A., Guinehut, S., & Morrow, S. (2012). A new estimate of the global 3D geostrophic ocean circulation based on satellite data and in-situ measurements. *Deep Sea Research Part II*, *77*, 70–81. https://doi.org/10.1016/j.dsr2.2012.04.012

Müller, T. J., & Siedler, G. (1992). Multi-year current time series in the eastern North Atlantic Ocean. *Journal of Marine Research*, *50*(1), 63–98. https://doi.org/10.1357/002224092784797755

Ni, Q., Zhai, X., Jiang, X., & Chen, D. (2021). Abundant cold anticyclonic eddies and warm cyclonic eddies in the global ocean. *Journal of Physical Oceanography*, *51*(9), 2793–2806. https://doi.org/10.1175/jpo-d-21-0010.1

Ni, Q., Zhai, X., Wang, G., & Hughes, C. W. (2020). Widespread mesoscale dipoles in the global ocean. *Journal of Geophysical Research: Oceans*, *125*(10), e2020JC016479. https://doi.org/10.1029/2020jc016479

Ni, Q., Zhai, X., Wang, G., & Marshall, D. P. (2020). Random movement of mesoscale eddies in the global ocean. *Journal of Physical Oceanography*, *50*(8), 2341–2357. https://doi.org/10.1175/jpo-d-19-0192.1

Petersen, M. R., Williams, S. J., Maltrud, M. E., Hecht, M. W., & Hamann, B. (2013). A three-dimensional eddy census of a high-resolution global ocean simulation. *Journal of Geophysical Research: Oceans*, *118*(4), 1759–1774. https://doi.org/10.1002/jgrc.20155

Rieck, J. K., Bning, C. W., Greatbatch, R. J., & Scheinert, M. (2015). Seasonal variability of eddy kinetic energy in a global high-resolution ocean model. *Geophysical Research Letters*, *42*(21), 9379–9386. https://doi.org/10.1002/2015gl066152

Scott, R. B., Arbic, B. K., Chassignet, E. P., Coward, A. C., Varghese, A., Merryfield, W. J., et al. (2010). Total kinetic energy in four global eddying ocean circulation models and over 5000 current meter records. *Ocean Modelling*, *32*(3–4), 157–169. https://doi.org/10.1016/j.ocemod.2010.01.005

Stammer, D. (1997). Global characteristics of ocean variability estimated from regional TOPEX/POSEIDON altimeter measurements. *Journal of Physical Oceanography*, *27*(8), 1743–1769. https://doi.org/10.1175/1520-0485(1997)027<1743:gcoove>2.0.co;2

van Aken, H. M., van Veldhoven, A., Veth, C., de Ruijter, W., van Leeuwen, P., Drijfhout, S., et al. (2003). Observations of a young Agulhas ring, Astrid, during MARE in March 2000. *Deep Sea Research II*, *50*(1), 167–195. https://doi.org/10.1016/s0967-0645(02)00383-1

Wunsch, C. (1997). The vertical partition of oceanic horizontal kinetic energy. *Journal of Physical Oceanography*, *27*(8), 1770–1794. https://doi.org/10.1175/1520-0485(1997)027<1770:tvpooh>2.0.co;2

Wunsch, C. (1999). Where do ocean eddy heat fluxes matter? *Journal of Geophysical Research*, *104*(C6), 13235–13249. https://doi.org/10.1029/1999jc900062

Wunsch, C. (2008). Mass and volume transport variability in an eddy-filled ocean. *Nature Geoscience*, *1*(3), 165–168. https://doi.org/10.1038/ngeo126

Wunsch, C., & Stammer, D. (1998). Satellite altimetry, the marine geoid, and the oceanic general circulation. *Annual Review of Earth and Planetary Sciences*, *26*(1), 2967–2973. https://doi.org/10.1146/annurev.earth.26.1.219

Xu, C., Zhai, X., & Shang, X. (2016). Work done by atmospheric winds on mesoscale ocean eddies. *Geophysical Research Letters*, *43*, 12174–12180.

Yang, Z., Zhai, X., Marshall, D. P., & Wang, G. (2021). An idealized model study of eddy energetics in the western boundary 'graveyard. *Journal of Physical Oceanography*, *51*(4), 1265–1282. https://doi.org/10.1175/jpo-d-19-0301.1

Yu, X., Ponte, A. L., Elipot, S., Menemenlis, D., Zaron, E. D., & Abernathey, R. (2019). Surface kinetic energy distributions in the global oceans from a high-resolution numerical model and surface drifter observations. *Geophysical Research Letters*, *46*(16), 9757–9766. https://doi.org/10.1029/2019gl083074

Zhai, X., Johnson, H. L., & Marshall, D. P. (2010). Significant sink of ocean-eddy energy near western boundaries. *Nature Geoscience*, *3*(9), 608–612. https://doi.org/10.1038/ngeo943

Zhang, Z., Wang, W., & Qiu, B. (2014). Oceanic mass transport by mesoscale eddies. *Science*, *345*(6194), 322–324. https://doi.org/10.1126/science.1252418

Zhang, Z., Zhang, Y., Wang, W., & Huang, R. X. (2013). Universal structure of mesoscale eddies in the ocean. *Geophysical Research Letters*, *40*(14), 3677–3681. https://doi.org/10.1002/grl.50736